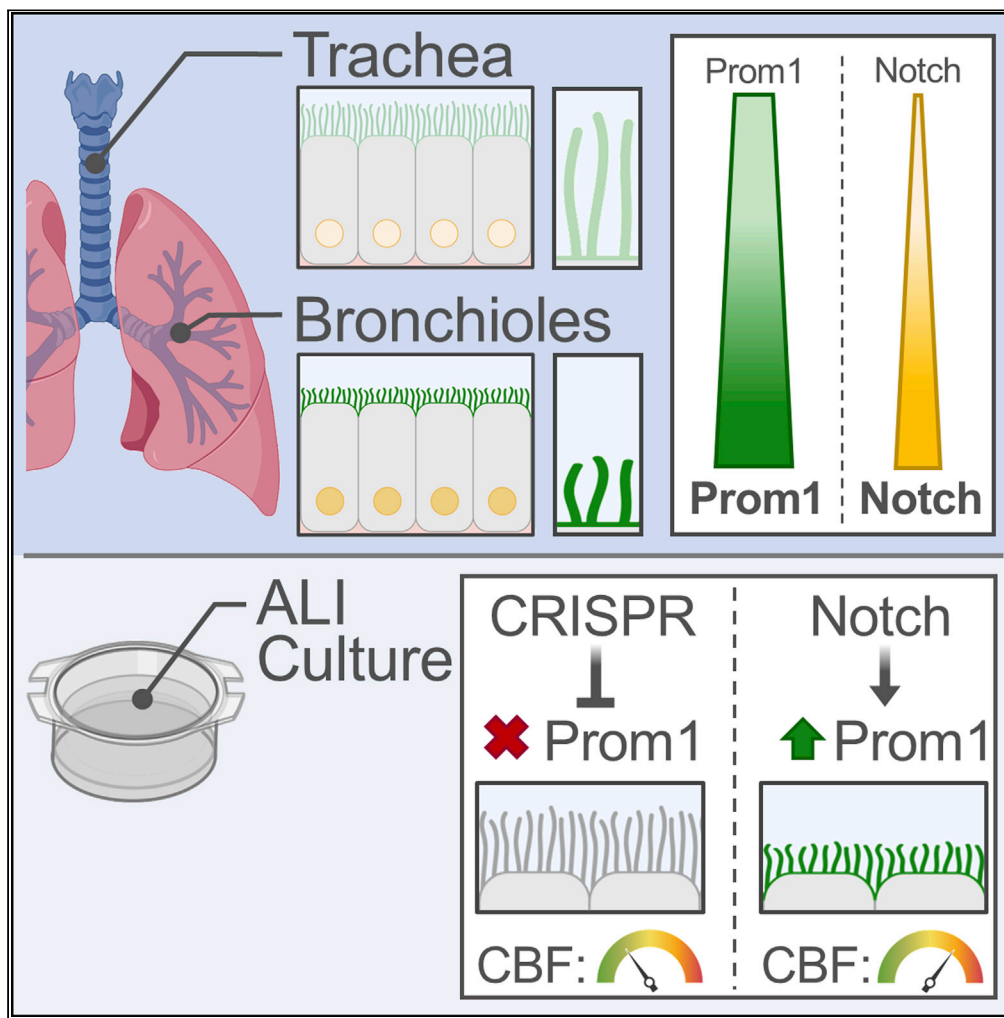


Article

Prominin 1 and Notch regulate ciliary length and dynamics in multiciliated cells of the airway epithelium



Carlos F.H. Serra,  
Helu Liu, Jun Qian,  
Munemasa Mori,  
Jining Lu,  
Wellington V.  
Cardoso

wvc2104@cumc.columbia.edu

Highlights

Prom1 is expressed in a proximal-distal gradient in developing airways

Prom1 is induced in post-specified multiciliated cells by low levels of Notch activation

Prom1 modulates cilia length and ciliary beating frequency in multiciliated cells

Notch fine-tunes Prom1 levels to generate multiciliated cell diversity in the airways

Serra et al., iScience 25,  
104751  
August 19, 2022 © 2022 The  
Authors.  
[https://doi.org/10.1016/  
j.isci.2022.104751](https://doi.org/10.1016/j.isci.2022.104751)

## Article

## Prominin 1 and Notch regulate ciliary length and dynamics in multiciliated cells of the airway epithelium

Carlos F.H. Serra,<sup>1,2,3</sup> Helu Liu,<sup>1</sup> Jun Qian,<sup>1</sup> Munemasa Mori,<sup>1</sup> Jining Lu,<sup>1</sup> and Wellington V. Cardoso<sup>1,4,\*</sup>

## SUMMARY

**Differences in ciliary morphology and dynamics among multiciliated cells of the respiratory tract contribute to efficient mucociliary clearance. Nevertheless, little is known about how these phenotypic differences are established. We show that Prominin 1 (Prom1), a transmembrane protein widely used as stem cell marker, is crucial to this process. During airway differentiation, Prom1 becomes restricted to multiciliated cells, where it is expressed at distinct levels along the proximal-distal axis of the airways. Prom1 is induced by Notch in multiciliated cells, and Notch inactivation abolishes this gradient of expression. Prom1 was not required for multicilia formation, but when inactivated resulted in longer cilia that beat at a lower frequency. Disruption of Notch resulted in opposite effects and suggested that Notch fine-tunes Prom1 levels to regulate the multiciliated cell phenotype and generate diversity among these cells. This mechanism could contribute to the innate defense of the lung and help prevent pulmonary disease.**

## INTRODUCTION

Cilia are highly conserved organelles formed by microtubule-based apical protrusions, the axonemes, that anchor to the cytoplasm via the basal bodies (Carvalho-Santos et al., 2011; Ishikawa and Marshall, 2011; Marshall, 2008). Nearly every cell has a single non-motile cilium, the primary cilium, critical for transducing cell-sensing signals (Singla and Reiter, 2006). By contrast, motile cilia have a more restricted tissue distribution and are usually found in epithelia that specialize in fluid movement, such as in the brain ventricles, the fallopian tubes, and the conducting airways of the respiratory system (Choksi et al., 2014). In these tissues, motile cilia are present in large numbers at the surface of multiciliated cells (100–200 per cell), often found interspersed with secretory cells (Horani and Ferkol, 2018; Tsao et al., 2009).

In the respiratory system, multiciliated cells are present throughout the entire air-conducting passages, from the trachea to the terminal bronchioles, where they are responsible for mucociliary clearance (Toskala et al., 2005). The synchronized beating of cilia across multiciliated cells continuously propels upward the mucous layer produced by the secretory cells, thus protecting the lungs against inhaled pollutants and pathogens. Along with the physical barrier formed by the tight junctions between epithelial cells, these mechanisms are essential components of the innate immunity (Knowles and Boucher, 2002). Disruption of these mechanisms by ciliary defects, such as ciliopathies, or by abnormal mucous production is frequently associated with respiratory infections and chronic obstructive pulmonary disease (Gohy et al., 2019; Mall, 2016).

Several studies have described regional differences in the phenotype and ciliary dynamics of multiciliated cells along the respiratory tract of the mammalian lung. Analysis of mucociliary clearance has shown a progressive decrease in the velocity of mucous transport across different generations of conducting airways from the trachea to the bronchioles (Polin, 2011). Multiciliated cells also display marked regional differences in ciliary length with longer cilia reported predominantly in the trachea and extrapulmonary bronchi when compared to those in the terminal bronchioles. These differences are already evident during late gestation, and suggest the influence of distinct local contexts during multiciliated cell differentiation (Toskala et al., 2005). Studies in immotile cilia have implicated a large number of pathways in the regulation of cilia assembly and growth (Keeling et al., 2016); however, less is known about the mechanisms generating phenotypical differences in the multiciliated cells of the airways.

<sup>1</sup>Columbia Center for Human Development, Department of Medicine, Pulmonary Allergy Critical Care, Department of Genetics and Development, Columbia University Medical Center, New York, NY 10032, USA

<sup>2</sup>Life and Health Sciences Research Institute (ICVS), School of Medicine, University of Minho, Braga, Portugal

<sup>3</sup>ICVS/3B's - PT Government Associate Laboratory, Braga/Guimarães, Portugal

<sup>4</sup>Lead contact

\*Correspondence: wvc2104@cumc.columbia.edu

<https://doi.org/10.1016/j.isci.2022.104751>



There is evidence that the Prominins, a family of transmembrane glycoproteins that localizes to plasmalemmal protrusions, including that of microvilli and cilia, influence ciliary morphology and function in different biological systems (Jaszai et al., 2020). Prominin 1 (Prom1, CD133) has been widely used as a stem cell marker in various tissues, and is considered to be a key marker of tumor-initiating cells in cancers. PROM1 is expressed in the adult human lung, with high levels reported in non-small-cell carcinomas associated with poor prognosis (Qiu et al., 2015). It is of particular interest that, in the adult lung, Prom1 is also found to be paradoxically expressed in the multiciliated cells of the airways, a cell type thought to be terminally differentiated (Rawlins and Hogan, 2008; Shmelkov et al., 2008; Travaglini et al., 2020). The association of Prominins with cilia appears to be well-conserved, as loss of function of these proteins results in various cilia-related phenotypes, including retinal degeneration and left-right asymmetry in non-mammalian species (Jaszai et al., 2020; Maw et al., 2000). Interestingly, some of the Prom1-related ciliary phenotypes have also been linked to defects in Notch signaling, a pathway involved in the development of both monociliated and multiciliated cells (Guo et al., 2019; Jaszai et al., 2020; Lopes et al., 2010). In fact, Prom1 and Notch are known to interact in different cell types and contexts to regulate cellular behaviors (Konishi et al., 2016). These observations raise intriguing questions about the functional significance of Prom1 in multiciliated cells, the processes mediated by Prom1 and Notch signaling, and their potential involvement in the generation of multiciliated cell diversity in the mammalian respiratory tract.

Here, we provide evidence that, during differentiation of the airway epithelium, Prom1 becomes restricted to multiciliated cells, where it is crucial in controlling cilia length and ciliary dynamics. Using mouse genetic approaches and functional assays in organotypic cultures, we show that Prom1 and Notch signaling regulate these features, ultimately establishing differences in morphology and function among multiciliated cells. Furthermore, we show that, by acting in multiciliated cells, Prom1 levels are key in the modulation of mucociliary clearance. Our results identify Prom1 as an integral regulator of the multiciliated cell function likely to contribute significantly to the innate defense mechanisms of the lung.

## RESULTS

### Prom1 becomes restricted to multiciliated cells in differentiating airway progenitors

Prom1 has been widely described as a stem cell marker, but has also been shown to be expressed in the differentiated epithelia of a variety of organs (Anderson et al., 2011; Fargeas et al., 2004; Florek et al., 2005). In a previous transcriptome analysis, we found Prom1 expression enriched in a population of non-secretory cells of late gestation lungs (below) (Guha et al., 2012). Despite having been reported in the developing lung (Weigmann et al., 1997), information about the Prom1 spatial and temporal patterns of expression was unavailable. We identified Prom1 expression uniformly distributed throughout the epithelium of the embryonic day 14.5 (E14.5) respiratory tract, from the trachea to the distal buds (Figures 1A and S1A). At this stage, the airway epithelium is still largely undifferentiated, thus suggesting that *Prom1* marked these cells at their progenitor stem-like state. *Prom1* transcripts were also detected in the epithelia of other developing tissues, including the kidney, brain, and intestine (Figure S1A). Immunofluorescence assays (IF) of the E14.5 airway epithelium further revealed the Prom1 subcellular localization restricted to the apical plasma membrane domain of the epithelial tubules (Figure 1A).

As the airway epithelium underwent differentiation, Prom1 was silenced in secretory cells while remaining strongly expressed in multiciliated cells. IF of E18.5 lungs showed Prom1 double-labeling with Foxj1, but not with the secretoglobin CC10 (Scgb1a1), established markers of multiciliated and secretory cells, respectively (Figures 1B and 1D). Confocal analysis of E18.5 airways showed still strong Prom1 subcellular localization at the base of cilia and apical plasma membrane of multiciliated cells; however, maximum projection views further revealed signals along the ciliary axonemes at this stage (Figure 1C). Intriguingly, at this stage, Prom1 labeling was not only restricted to multiciliated cells, but its signal intensity was regionally distinct throughout the respiratory tract epithelium. Plotting of the mean fluorescence intensity of individual multiciliated cells from different airway generations of a single section of E18.5 lungs showed a gradient of Prom1 expression along the proximal-distal axis of the airways, with lower levels in the trachea and increasing signal intensity in intrapulmonary airways (Figure 1F). Prom1 signals are maintained in multiciliated cells of the adult lung with signals in small intrapulmonary airways still stronger than in the trachea; however, this graded expression is less obvious compared to that in embryonic lungs.

We asked whether Prom1 could have a similar cell type restriction during the differentiation of adult airway progenitors. Thus, we isolated airway basal cells from adult murine tracheas and expanded them to confluency

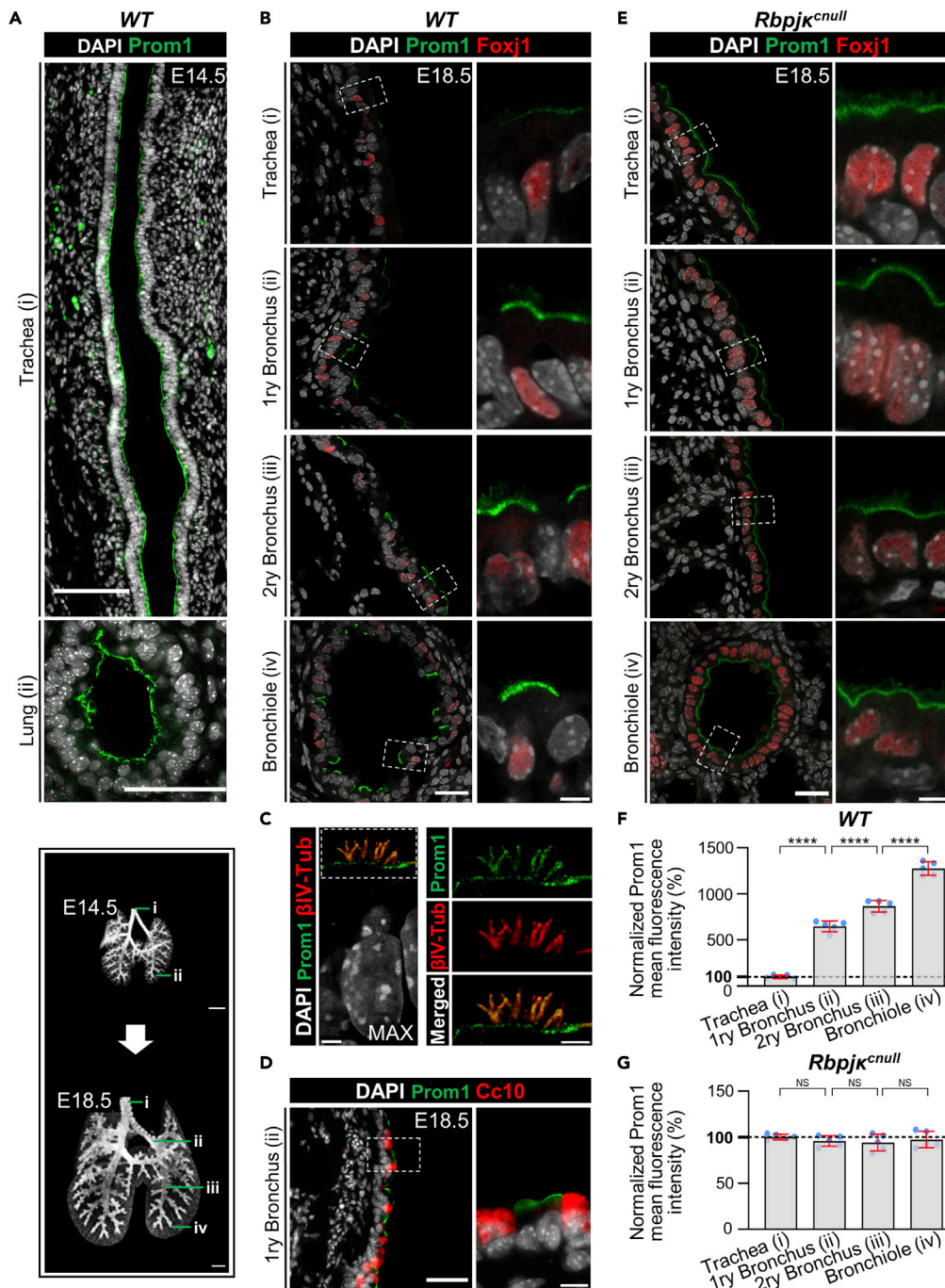


**Figure 1. Prom1 becomes restricted to multiciliated cells and its regional levels are controlled by Notch signaling in the developing lung**

(A) Immunofluorescence (IF) of Prom1 in the E14.5 trachea and intrapulmonary airways at the sites indicated by the numbered green bars in the diagram at the bottom left (adapted from Alanis et al. (2014), depicting the stages analyzed in panels A–D, E). Prom1 is detected throughout the epithelium at the apical surface.

(B) Double Prom1/Foxj1 IF in E18.5 wild-type lungs. Each panel represents a series of single optical sections from different airway generations as depicted in the diagram (Boxed areas enlarged on the right panels). Prom1 is detected in multiciliated cells marked by Foxj1; labeling is stronger in intrapulmonary airways.

(C) Maximum intensity projection of double Prom1/βIV-Tubulin in E18.5 WT lungs. Boxed area is enlarged on the right panels. Prom1 is detected in ciliated cells in the apical membrane, and in the axonemes where it co-localizes with βIV-Tubulin.

**Figure 1. Continued**

(D) Double IF of Prom1/Cc10 in E18.5 wild-type lungs. Boxed areas are enlarged on the right panel. Prom1 is not detected in secretory cells (marked by Cc10).

(E) Double Prom1/Foxj1 IF in E18.5 *Rbpjk<sup>cnull</sup>* lungs in different airway generations as depicted in diagram (green bars, bottom left). Boxed areas are enlarged on the right panels. The intensity of the Prom1 channel was increased in relation to panel B in order to better visualize the signal. Airways are overpopulated by multiciliated cells uniformly labeled by Prom1.

(F) Graph: Prom1 mean fluorescence intensity in different airway generations of E18.5 wild-type lungs. The beeswarm plot represents the mean fluorescence intensity of individual cells compared to trachea (\*, N = 5). Bars represent the mean  $\pm$  SD. Prom1 proximal-distal gradient with higher expression in bronchioles. Sidak's multiple comparisons test: \*\*\*\*,  $p < 0.0001$ .

(G) Graph: Prom1 mean fluorescence intensity in different airway generations of E18.5 *Rbpjk<sup>cnull</sup>* lungs. The beeswarm plot represents the mean fluorescence intensity of individual cells from each airway generation compared to the trachea (\*, N = 5). Bars represent the mean  $\pm$  SD. No gradient of Prom1 expression in multiciliated cells along the proximal-distal axis of *Rbpjk<sup>cnull</sup>* airways. Sidak's multiple comparisons test: NS, not significant. DAPI is gray in all panels. 1ry = Primary; 2ry = Secondary. Scale bars in A (top and bottom panels) = 100 and 50  $\mu$ m (respectively); in the diagram (top and bottom panels) = 400 and 500  $\mu$ m (respectively); in B (left and right panels) = 25 and 5  $\mu$ m (respectively); in C (left and right panels) = 2.5  $\mu$ m; in D (left and right panels) = 50 and 10  $\mu$ m (respectively); and in E (left and right panels) = 25 and 5  $\mu$ m (respectively).

in Transwell cell culture plates, as previously reported (You and Brody, 2013). IF-confocal microscopy showed Prom1 expressed uniformly in all basal cells, largely at the apical surface, a pattern reminiscent of that found in the progenitors of the developing E14.5 airway epithelium *in vivo* (Figures S1B and 1A). Analysis of these cultures differentiating under air-liquid interface (ALI) conditions showed Prom1 selectively detected in multiciliated cells, as confirmed by the co-labeling with  $\beta$ -IV Tubulin (Figure S1C). Notably, these cells displayed a great degree of heterogeneity in regards to Prom1 expression, as seen by the wide range of labeling intensities throughout the culture period (Figures S1C and S1D). We reasoned that this could be ascribed to potential differences in the stage of differentiation of the multiciliated cells arising in the same culture (timing), or to the presence of progenitor cells cultured from distinct regions of the trachea (spatial heterogeneity). The fact that the differences in Prom1 expression persisted in later-stage cultures, when multiciliated cells were nearly all mature (ALI day 27) (Figure S1D), suggested that the heterogeneity we observed reflected intrinsic differences in the developmental program of these progenitors associated with their original location. Overall, these results revealed a conserved pattern of restriction of Prom1 expression as cells transition from an undifferentiated stem-like status to a highly differentiated multiciliated cell lineage both in the developing lung and in the adult airways differentiating *in vitro*. They also underscored the substantial heterogeneity of multiciliated cells in regards to Prom1 expression, both *in vivo* and *in vitro*.

**Notch signaling controls local and regionally distinct levels of Prom1 in multiciliated cells**

To gain additional insights into the heterogeneity of multiciliated cells of the airway epithelium, we examined lungs from mouse mutants in which these cells had been massively expanded by disruption of Notch signaling. Notch regulates cell fate decisions in the developing airways by fostering the secretory cell fate and preventing excessive multiciliated cell differentiation (Tsao et al., 2009). Analysis of E18.5 mutants in which we inactivated canonical Notch signaling early in the lung epithelium (*ShhCre; Rbpjk<sup>ff</sup>*, hereafter *Rbpjk<sup>cnull</sup>*) showed the expected expansion of multiciliated cells in the airways (Figure S3) (Tsao et al., 2009, 2011). Notably, Prom1/Foxj1 double-IF staining of E18.5 *Rbpjk<sup>cnull</sup>* lungs not only showed airways massively overpopulated by double-labeled multiciliated cells but also revealed an overall low uniform pattern of Prom1 expression in multiciliated cells throughout the extra- and intrapulmonary airways (Figures 1 and S3A). Plotting of the mean Prom1 fluorescence intensity of individual multiciliated cells from different airway generations of E18.5 mutant lungs showed similar values along the proximal-distal axis, in contrast to the graded distribution seen in wild-type (WT) lungs (Figures 1F and 1G). Thus, disruption of Notch signaling altered Prom1 expression within these cells, attenuating the normal gradient observed in WT lungs. We examined whether a similar gradient of Notch activation existed in multiciliated cells from large to small airways. Nuclear localization of Notch intracellular domain (NICD) is well known as a hallmark of secretory cells in the luminal airway epithelium. Our confocal analysis of E18.5 lungs confirmed this observation but also revealed low levels of NICD in multiciliated cells throughout the airways. Notably, triple NICD, Foxj1, and Prom1 IF showed differential levels of NICD expression with the strongest signals in multiciliated cells of distal/small intrapulmonary airways and nearly no expression in these cells at the trachea (Figure S2). Transcriptome profiling of E18.5 *Rbpjk<sup>cnull</sup>* lungs showed a significant increase in the expression of Foxj1 and other cilia-associated genes, compared to wild-type controls, consistent with

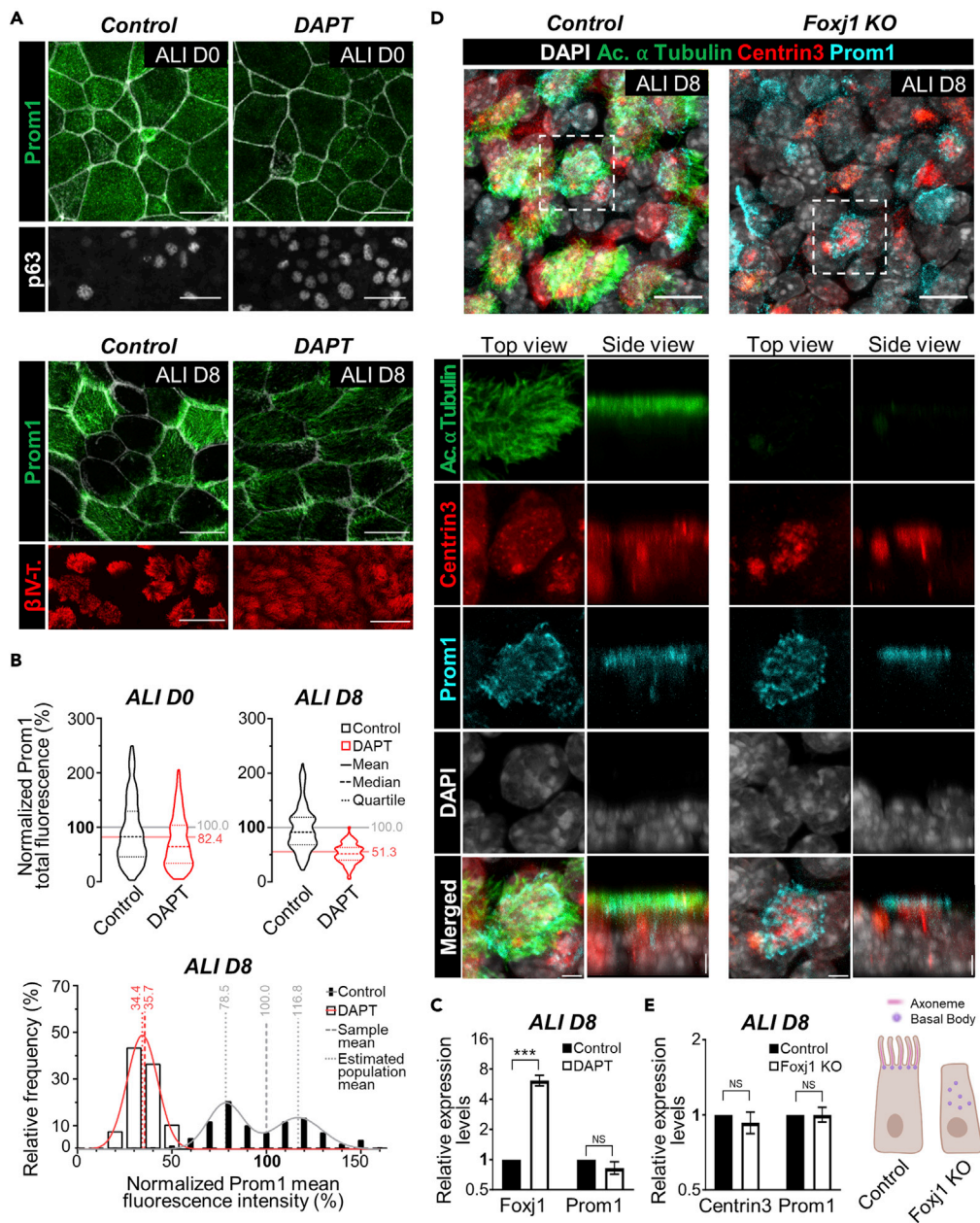


**Figure 2. Prom1 expression is dependent on endogenous Notch signaling in multiciliated cells and independent of multicilia formation**

(A) Immunofluorescence (IF) of Prom1, p63, and acetylated  $\alpha$ -tubulin in control and DAPT-treated ALI airway cultures at days 0 and 8. Expansion of the basal (p63+) and multiciliated ( $\beta$ tubulin+) cell population. Prom1 expression decreased by DAPT. Prominent heterogeneity of Prom1 signals in control ALI day 8 compared to day 0 (Phalloidin shown in gray in top panels).

(B) Top panels: Violin plots representing the distribution of the single-cell total Prom1 fluorescence, normalized by fluorescent phalloidin, and so that the mean total fluorescence of the control conditions equal 100%. Total fluorescence was calculated from the integrated density (mean gray value  $\times$  cell area) measured from the sum of multiple Z-slices encompassing the whole thickness of the cell layer. The solid lines represent the mean, the dashed lines represent the median, and the dotted lines represent the quartiles. The total fluorescence of Prom1 per cell is slightly decreased in Notch-deficient conditions at day 0 ( $\approx$ 82% of control), and even more at day 8 ( $\approx$ 51% of control). Bottom panel: Bar chart representing the frequency distribution of the multiciliated single-cell mean Prom1 fluorescence normalized by fluorescent phalloidin. Mean fluorescence was measured from the sum of multiple Z-slices encompassing the whole thickness of the cell layer. The solid lines represent non-linear curve fittings for the frequency distribution, the dashed lines represent

**Figure 2. Continued**

the average of each sample, and the dotted lines represent the means of the fitted Gaussian curves. At day 8, the solid gray line represents the sum of two Gaussian curves (Mean  $\pm$  SD of  $78.48 \pm 9.48\%$  and  $116.8 \pm 12.81\%$ ,  $R^2 = 0.9541$ ), and the solid red line represents a single Gaussian curve (Mean  $\pm$  SD of  $34.41 \pm 8.08\%$ ,  $R^2 = 0.9929$ ). The fitted curve for the mean fluorescence of Prom1 per multiciliate cell at day 8 suggests the presence of multiple normally distributed populations in control cultures, but only a single one in Notch-deficient cultures.

(C) qPCR analysis of Foxj1 and Prom1 in control and DAPT-treated day 8 ALI cultures (N = 3). Foxj1 expression was increased 6-fold in DAPT-treated ALI, yet there was no significant difference in the expression of Prom1. Graph represents fold change  $\pm$  CI95 on a log2 scale. Student's t-test: \*\*\*,  $p < 0.001$ ; ns, not significant.

(D) Triple IF of Prom1, acetylated  $\alpha$ -tubulin, and Centrin3 in ALI day 8 cultures incubated with CRISPR/Cas9 lentiviral vectors carrying a scrambled-sequence (Control, left panels) or a Foxj1-targeting sequence (Foxj1 KO, right panels). Top and side views of the boxed areas are enlarged in bottom panels for each marker. All panels represent maximum intensity projections. In Foxj1 KO cultures, the ciliated cell fate is specified but multiciliogenesis does not occur; Prom1 expression is unaffected and still limited to the apical region of multiciliated-fated cells (marked by Centrin3). DAPI is gray in all panels.

(E) qPCR analysis of Prom1 and Centrin3 in Control and Foxj1 KO day 8 ALI cultures (N = 3). There is no significant difference in Prom1 and Centrin3 in Foxj1 KO. Graph represents fold change  $\pm$  CI95 on a log2 scale. Student's t-test: ns, not significant. Scale bars in A = 25  $\mu$ m, and in D (top and bottom panels) = 10 and 2.5  $\mu$ m (respectively).

the underlying overpopulation of multiciliated cells. However, the massive increase in these cells was accompanied by only a modest increase in Prom1 even though this gene was found selectively expressed in multiciliated cells (Figure S3B). This suggested that, in a per cell basis, Prom1 expression, rather than increased, was actually decreased by Notch loss of function. Indeed, in a similar analysis of E18.5 mice in which Notch signaling was constitutively activated in the developing lung epithelium (ShhCre; NICD), we found a marked increase in Prom1, in stark contrast to the decrease in expression of the other cilia-associated genes (Figure S3B) in these lungs. Together, these observations were compatible with Notch being a positive regulator of Prom1 in differentiated multiciliated cells.

To examine whether Notch also influenced the program of Prom1 expression in adult progenitors undergoing multiciliated cell differentiation, we cultured basal cells isolated from adult WT murine tracheas (as above) and disrupted Notch signaling pharmacologically with the gamma-secretase inhibitor DAPT (Geling et al., 2002). Efficient Notch inhibition was confirmed by the expansion of basal cells in ALI day 0 and by excessive multiciliated cell differentiation at ALI day 8 (Mori et al., 2015). DAPT treatment resulted in Prom1 signals slightly decreased at day 0 compared to controls, but by day 8 Prom1 expression had sharply declined in the DAPT cultures (Figure 2A). We quantified the total fluorescence in Prom1-expressing basal cells. Our results indicated that cells from DAPT-treated cultures at ALI day 0 had approximately 80% of the total Prom1 fluorescence measured in the respective control, and that this value further decreased to approximately 50% by ALI day 8 (Figure 2B). In addition, the Prom1 signals in multiciliated cells from day 8 DAPT-treated cultures seemed more uniform across all multiciliated cells compared to the variable Prom1 levels in these cells from controls (Figures 2A and S1C). To further examine this possibility, we compared the frequency distribution of the mean Prom1 fluorescence intensity of individual multiciliated cells from control and Notch-deficient cultures at day 8. Our analysis confirmed that, in the control cultures, the mean fluorescence of Prom1 was indeed not uniform across the multiciliated cell population. Furthermore, it showed that a sum of two Gaussian curves ( $R^2 = 0.9541$ ) fitted the frequency distribution better than a single Gaussian curve ( $R^2 = 0.7273$ ), thus suggesting the underlying presence of at least two distinct multiciliated populations based on differences in Prom1 expression. By contrast, in DAPT-treated cultures, the frequency distribution had a single peak whose mean was approximately 35% of the fluorescence intensity of the control. This was consistent with the presence of a single, more uniform multiciliated cell population with lower levels of Prom1 expression (Figure 2B). Thus, disruption of Notch not only decreased Prom1 levels but also led to the appearance of a more uniform population of Prom1<sup>low</sup> cells. Taken together, these results show that multiciliated cells in the airway epithelium differ in their ability to express Prom1. This appears to depend on their distinct local or regional contexts in the respiratory tract *in vivo* and *in vitro*, as they were observed in E18.5 lungs and in adult organotypic cultures. These differences seem to also depend on Notch signaling, suggesting that this pathway is differentially activated in subpopulations of multiciliated cells.

**Prom1 is not required to initiate multiciliogenesis, and its expression in multiciliated cells is not dependent on the formation of axonemes**

Our data showed that, during airway epithelial differentiation, Prom1 expression is selectively maintained in the cells committed to initiate the program of multiciliogenesis. This led us to examine whether

preventing subsequent events of the ciliogenesis program in cells fated to become multiciliated would have any impact in Prom1 expression and localization. Foxj1 is a transcription factor crucial for basal body docking and initiation of multiciliogenesis (Brody et al., 2000). We employed a CRISPR/Cas9 gene-editing approach to disrupt the expression of Foxj1 in airway progenitors *in vitro*. A lentiviral vector carrying an sgRNA targeting Foxj1, Cas9, and a puromycin resistance gene was used to create double-stranded breaks in the Foxj1 coding sequence of airway progenitors, ultimately resulting in the knockdown of functional Foxj1 protein in ALI cultures (Figure S4A). A lentiviral vector containing a scrambled sgRNA sequence was used as control.

Freshly isolated adult airway progenitors were incubated with lentivirus-containing medium for 48 h. Transduced cells were selected by puromycin resistance, expanded to confluency, and finally differentiated under ALI conditions for 8 days, as previously reported by Horani et al. (2013). Efficient knockdown of Foxj1 was demonstrated by qPCR and cytometry analyses, with both showing a significant decrease in Foxj1 expression when compared to controls (Figures S4B and S4C). Disruption of Foxj1 expression resulted in the expected loss of acetylated  $\alpha$ -tubulin-labeled axonemes characteristic of multiciliated cells. Nonetheless, the multiciliated identity of these cells could still be readily recognized by the abundant expression of Centrin3, which labels the multiple basal bodies that remained undocked in the absence of functional Foxj1 (You et al., 2004) (Figure 2C). Remarkably, IF of Foxj1-disrupted cultures showed Prom1 expression still limited to the Centrin3+ cells, which were committed to the multiciliated cell fate. Furthermore, Prom1 apical localization remained unaffected in spite of the defect in basal body docking and the consequent lack of cilia (Figure 2C). Morphometric and qPCR analyses revealed no significant differences in the expression levels of *Prom1* and *Centrin3* in Foxj1-deficient cultures when compared to controls (Figure 2D). Together, these results indicate that, although in the airway epithelium Prom1 is normally restricted to multiciliated cells, its expression and apical subcellular localization do not depend on basal body docking or on the elongation of axonemes.

### Disruption of Prom1 results in multiciliated cells with overly elongated cilia

Previous studies in *Prom1*<sup>-/-</sup> mice have reported complex phenotypes, with varying severities depending on the genetic background. Some of the abnormalities include: retinal degeneration (Dellett et al., 2014), spermatogenesis defects, abnormal intestinal-crypt proliferation and inflammation (Karim et al., 2014), and tooth developmental defects (Singer et al., 2019), among others. No information was available regarding the impact of Prom1 deletion in the airway epithelium. To gain insights specifically into this issue and circumvent the systemic effects of *Prom1*<sup>-/-</sup> mice, we disrupted Prom1 expression in airway epithelial progenitors from adult mouse tracheas using a similar CRISPR/Cas9 approach (described above). Efficient disruption of Prom1 expression in airway progenitors was confirmed by qPCR, Western blot, and IF analyses (Figures S5A–S5C). Immunostaining for p63, a transcription factor that marks the airway basal cells (Rock et al., 2009), indicated that the loss of Prom1 did not have any impact in the relative abundance of this population, nor in their ability to expand and form a confluent cell layer (Figure S5D). Confluence was reached just as fast in Prom1-CRISPR/Cas9-targeted (KO) cultures as it was in controls. Next, we examined the phenotype of multiciliated cells derived from the Prom1-deficient progenitors in ALI cultures. Loss of Prom1 had no effect in the balance of multiciliated vs secretory cells. We did not find significant differences in the relative expression levels of *Centrin3* and *Scgb3a2*, or in the number of Centrin3-labeled cells, when compared to controls (Figures 3 and S6). Analyses of fully differentiated cultures at a later stage (ALI day 27) showed a marked increase in cilia length in multiciliated cells from Prom1-deficient cultures compared to controls. XZ optical-reconstructions from confocal laser scanning micrographs identified long, Prom1-negative, acetylated  $\alpha$ -tubulin-labeled axonemal structures (Figure 3A). Morphometric analysis of cilia from scraped multiciliated cells, using an established method based on high-speed video microscopy (HSVM) recordings of live cells (see STAR Methods) (Oltean et al., 2018), confirmed the increase in cilia length (CL) of multiciliated cells from Prom1-deficient cultures when compared to controls (Prom1 KO:  $5.93 \pm 0.19 \mu\text{m}$  vs. Control:  $5.33 \pm 0.22 \mu\text{m}$ ; p value = 0.0235) (Figure 3B).

### Ciliary beating and mucociliary transport are impaired in Prom1-deficient airways

Our analysis showed that the disruption of Prom1 expression in airway progenitors had no impact in their ability to undergo multiciliogenesis. However, it was unclear whether the abnormally long cilia found in Prom1-deficient ALI were still functional and able to beat at frequencies comparable to those found in control cultures. To investigate this, we recorded HSVM videos of live, fully differentiated (ALI day 27) airway epithelial cultures that had been transduced with either a control, or a Prom1-inactivating lentiviral vector.

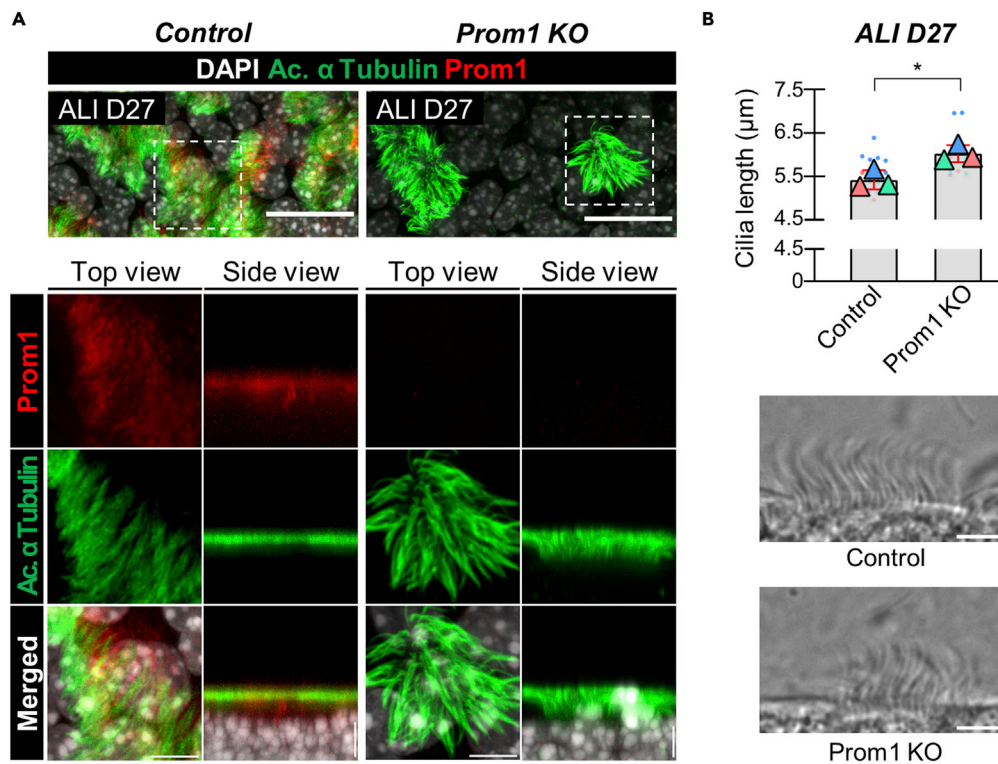


**Figure 3. Disruption of Prom1 increases ciliary length (CL) in multiciliated cells**

(A) Double immunofluorescence of Prom1 and acetylated  $\alpha$ -tubulin in ALI day 27 cultures incubated with CRISPR/Cas9 lentiviral vectors carrying a control (left panels) or Prom1-targeting sequence (Prom1 KO, right panels). Top and side views of the boxed areas are enlarged in bottom panels. All panels represent maximum intensity projections. Prom1 KO does not prevent multiciliated cell differentiation but results in increased cilia length.

(B) Cilia length analysis from multiciliated cells of control and Prom1 KO ALI day 27 cultures. Top: beeswarm plot of the average cilia length of each multiciliated cell ( $\bullet$ ,  $\bar{N} \approx 6$ ) and well ( $\Delta$ ,  $N = 3$ ) superimposed on a bar chart representing the sample-mean  $\pm$  SD. The original values were measured by averaging the length ( $\mu\text{m}$ ) of five individual cilia from each multiciliated cell ( $N_{\text{Cilia}} = 5$ ). Cilia length is increased in multiciliated cells from Prom1 KO cultures. Bottom: single, representative video frames for the conditions tested. Student's t-test: \*, p value  $< 0.05$ . DAPI is gray in all panels. Scale bars in A (top and bottom panels) = 20 and 5  $\mu\text{m}$  (respectively), and in B = 5  $\mu\text{m}$ .

The cells were imaged *en face* while still attached to the membranes, in 25 random fields per well, at a frame rate of 360 frames per second and at stable temperature of 37°C, as described by Oltean et al. (2018). The fast Fourier transform (FFT) was used to calculate the ciliary beating frequency (CBF) from the movement detected for each individual pixel of a video frame. Prom1-deficient multiciliated cells showed significantly lower CBF compared to controls (Prom1 KO:  $37.52 \pm 2.17$  Hz vs. Control:  $42.46 \pm 1.78$  Hz, p value = 0.0457). Thus, disruption of Prom1 in airway progenitors resulted in multiciliated cells with increased cilia length and lower frequencies of ciliary beating (Figure 4A).

Since both ciliary morphology and dynamics differ along generations of airways *in vivo* and both were significantly altered in Prom1 KO cultures, we examined whether, under control conditions, differences in CL among multiciliated cells are necessarily accompanied by corresponding changes in CBF. CBF and CL were measured together in HSVM recordings of multiciliated cells from control ALI day 27 cultures. Pearson's correlation analysis showed no significant correlation between CL and CBF ( $|r| = -0.3521$ ,  $p = 0.0994$ ) (Figure S7), in agreement with similar observations in ALI organotypic cultures from human donors (Oltean et al., 2018). This suggested that the changes in ciliary length and dynamics mediated by Prom1 are unlikely to be interdependent and possibly result from Prom1 acting in multiciliated cells through different mechanisms.

Our analysis of airway organotypic ALI cultures showed Prom1 selectively expressed in multiciliated cells already early during differentiation. However, it was unclear when Prom1 started to influence CBF in these

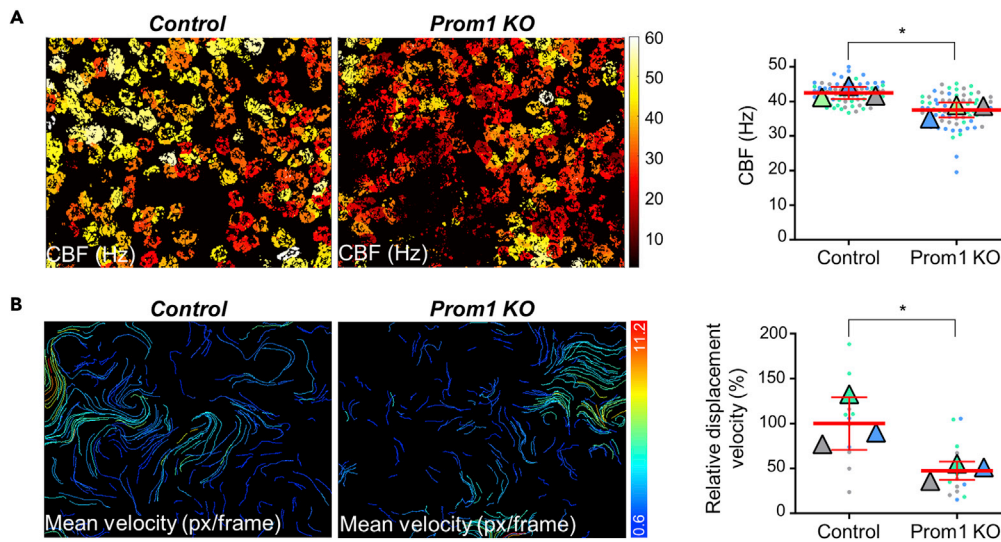


**Figure 4. Loss of Prom1 impairs ciliary beating and mucociliary transport**

(A) Analysis of ciliary beating frequency (CBF) in ALI day 27 cultures incubated with CRISPR/Cas9 lentiviral vectors carrying control or Prom1 KO sequences. The heatmaps on the left depict the CBF values of each pixel from representative recordings of control and Prom1 KO cultures. The graph on the right represents a beeswarm plot of the average CBF (Hz), of each video ( $\bullet$ ,  $N = 25$ ) and well ( $\Delta$ ,  $N = 3$ ), with the sample-means  $\pm$  SD superimposed in red. Prom1 KO cultures had a significantly lower CBF compared to control. Student's t-test: \*, p value  $<0.05$ .

(B) Mucociliary transport (MCT) in ALI day 27 cultures incubated with CRISPR/Cas9 control or Prom1 KO vectors. The heatmaps on the left depict the mean displacement velocity values of each fluorescent microsphere's track, in pixel/frame, from representative recordings of control and Prom1 KO cultures. The graph on the right represents a beeswarm plot of the relative mean-displacement velocity weighted according to displacement distance of each respective track, of each video ( $\bullet$ ,  $N = 5$ ) and well ( $\Delta$ ,  $N = 3$ ), normalized so that the mean velocity of control = 100%, and with the sample-mean  $\pm$  SD superimposed in red. Microspheres from Prom1 KO cultures had a significantly lower displacement velocity when compared to control. Student's t-test: \*, p value  $<0.05$ .

cells. Thus, we performed HSVM recordings in Prom1 KO cultures at different stages to investigate when Prom1 deficiency first altered ciliary dynamics. We found no difference in CBF in Prom1-deficient ALI cultures at day 8 when compared to controls. However, two days later, CBF was first significantly decreased in Prom1 KO cultures. Interestingly, in a similar analysis of CBF in ALI cultures treated with DAPT, we found CBF significantly increased compared to controls already at day 8, suggesting that Notch acts on CBF even before Prom1, presumably through a Prom1-independent mechanism (Figure S8).

To better understand the functional implications of Prom1 disruption in the airway epithelium, we assessed Mucociliary Transport (MCT) by tracking the displacement of fluorescent microspheres added to the surface of ALI cultures, as described by Oltean et al. (2018). Briefly, fluorescent microspheres were added to the surface of ALI day 27 cultures and HSVM recordings were performed which allowed us to track the displacement of individual microspheres, and subsequently determine the displacement distance (in pixels) and displacement velocity (in pixels/frame) using the TrackMate software (Tinevez et al., 2017). The final MCT value for each video was calculated by weight-averaging the displacement velocity of every track by their respective displacement distance. This analysis revealed a significant impairment of MCT in Prom1-deficient cultures (Prom1 KO Mean  $\pm$  SD =  $47.61 \pm 10.09\%$ , p value = 0.0423) (Figure 4B). Together, these results indicate that Prom1 influences various aspects of the multiciliated cell phenotype and behavior, which ultimately contribute to the efficiency of MCT. These observations place Prom1 as a relevant regulator of the multiciliated cell phenotype, and one who is likely to have a significant impact in the defense mechanisms of the airway epithelium.

## DISCUSSION

Here, we provide evidence of Prom1 acting as a key regulator of the ciliary structure and function in multiciliated cells of the murine respiratory tract. We identified Prom1 widely distributed in the undifferentiated

airway progenitors of both the developing and adult lungs, and becoming restricted to multiciliated cells as differentiation takes place. Our findings of distinct levels of Prom1 in multiciliated cells raised the possibility that the diversity of these cells is in part mediated by differential expression of Prom1. Our loss-of-function analyses showed that while Prom1 is not required for initiation of multiciliogenesis, it influences ciliary length. The data suggest that Prom1 operates with Notch signaling in the generation of multiciliated cell diversity in the developing and adult airways. Furthermore, we show that Prom1 contributes to generate functional differences among multiciliated cells by regulating ciliary dynamics, in a process likely independent of cilia length.

The precise mechanism by which Prom1 controls ciliary length in the airway epithelium is still unclear. Interestingly, analyses of mouse embryos during neurogenesis identified Prom1 in the plasmalemmal protrusions of primary cilia from neuroepithelial cells. The presence in the neural tube fluid of Prom1-rich membrane particles containing alpha tubulin suggests that cilia length could be controlled by shedding of Prom1-rich membrane domains (Dubreuil et al., 2007). This mechanism is likely to be relevant in multiple biological contexts, since Prom1-containing membrane particles have been identified in a variety of body fluids, including urine, saliva, and seminal fluids (Marzesco et al., 2005). Preliminary data suggest that these particles are also present in the mucous layer of our airway ALI cultures, and ongoing work is focusing on how to accurately detect and quantify them. Future work will include correlating the rate of shedding of Prom1 particles with changes in cilia length in conditions such as Prom1 deletion and cilia damage by environmental (smoke) exposure. Moreover, the analysis of Prom1 particles in human airway secretions could potentially be valuable as an indirect approach to assess cilia damage. Studies in Madin-Darby canine kidney (MDCK) cells in which specific domains of Prom1 had been mutated suggest that the effect of Prom1 in cilia length can also involve interactions with ADP-ribosylation factor-like protein 13B (Arl13b), as well as cross-talking with cytoskeleton regulators in the cellular membrane microenvironment (Jaszai et al., 2020). Similar mechanisms could potentially be in place in airway-multiciliated cells.

The relationship between Notch signaling and Prom1 expression is intriguing. Notch-Prom1 interactions have been reported in various cellular contexts: Notch signaling has been shown to positively regulate Prom1 expression in human breast cancer cells (Sansone et al., 2017), and in different types of gastric cancer cells, specifically through an RBPJK-dependent pathway (Konishi et al., 2016). Considering our detection of nuclear NICD in multiciliated cells and that Notch signaling is known to prevent the differentiation of airway progenitors into multiciliated cells, we propose that once airway progenitors have been committed to the multiciliated cell fate and ciliogenesis has initiated, subtle levels of Notch activation in multiciliated cells regulate the expression of cilia-related genes, such as Prom1, thereby influencing ciliary morphology and function. This is supported by various lines of evidence: Notch signaling is active and required to maintain proper ciliary length of the motile cilia in the zebrafish left-right organizer, with Notch inactivation resulting in shortened cilia and severe laterality defects in the embryo (Lopes et al., 2010); Notch activity in the murine-developing neural tube has been shown to produce longer primary cilia (Stasiulewicz et al., 2015). We have evidence that this is also true in differentiating multiciliated cells as seen by the decreased cilia length in ALI organotypic cultures in which Notch was inactivated in Rbpjk<sup>fl/fl</sup> adult progenitors transduced using a lentivirus-expressing Cre approach (Figure S9).

Notably, a recent comprehensive single-cell RNAseq-based survey of the cellular components of the human lung identified two regionally distinct populations of multiciliated cells that differ in their location and molecular signature: “proximal ciliated”, and “ciliated”. Further analysis of the published database (Synapse [<https://www.synapse.org/#!Synapse:syn21041850>]; cellxgene at <https://hlca.ds.czbiohub.org>) revealed that these populations differentially express Notch receptors (NOTCH1 and NOTCH2) and the Notch target HES1, all of which are particularly enriched in the multiciliated “non-proximal” cell population (Travaglini et al., 2020). This is in accordance with our concept of multiciliated cells differing in their ability to express and activate Notch. We further hypothesize that this variable activation of Notch is likely to result in regional differences in the expression of target genes such as Prom1, which may in turn contribute to the observed differences in the multiciliated cell phenotype along the respiratory tract.

Ultimately, we propose that Prom1 and Notch signaling are part of a putative mechanism responsible for maintaining the proper structure and function of motile cilia in the multiciliated cells throughout the airway epithelium. Our observations of the graded Prom1 expression *in vivo* suggest that Prom1 is deliberately kept at different regional levels, and that the higher levels of Prom1 in the small intrapulmonary airways

may help to prevent the formation of inappropriately long and/or fast-beating cilia. We show in our airway epithelial culture system that the lack of Prom1 expression not only results in longer, slower-beating cilia, but also has a negative impact in mucociliary transport. By influencing aspects such as ciliary length and dynamics, this mechanism would contribute to generate heterogeneity among multiciliated cells from different airway generations, and thus have an impact in the overall diversity of this cell type. The Prom1 regulation of the ciliary phenotype can be relevant during the repair of damaged, shortened cilia that results from exposure to cigarette smoke and biological agents, and ultimately failed in chronic pulmonary conditions, such as COPD (Leopold et al., 2009). Lastly, we also consider that the mechanisms described here may be relevant in the context of multiciliated cells in other mammalian organs, including that of the reproductive tract.

### Limitations of the study

A potential limitation of our study was that the *in vivo* transcriptome analyses of Notch mutants were performed in bulk rather than by single-cell RNAseq. Thus, a more precise analysis of the gene expression signature of the different subpopulations of multiciliated cells could not be obtained with our approach. However, this was unlikely to have had a major impact in our conclusions since the changes in gene expression identified in these mutants resulted from a clear phenotype in which the balance of secretory and multiciliated cells in the airway epithelium was profoundly altered. Our protocol of pharmacological inactivation of Notch with DAPT was highly efficient in the analysis of the early stages of multiciliogenesis. However, some pleiotropic effects observed in long-term ALI organotypic cultures made it less suitable to assess late stages of maturation of the airway epithelium. The reasons are still unclear to us. This also precluded the analysis of Notch inhibition in late stage fully mature Prom1 KO cultures.

### STAR★METHODS

Detailed methods are provided in the online version of this paper and include the following:

- KEY RESOURCES TABLE
- RESOURCE AVAILABILITY
  - Lead contact
  - Materials availability
  - Data and code availability
- EXPERIMENTAL MODEL AND SUBJECT DETAILS
  - Mouse models
  - Air-liquid-interface (ALI) organotypic airway epithelial cultures
- METHOD DETAILS
  - Immunofluorescence (IF)
  - Cytometry and fluorescence intensity analyses
  - *In situ* hybridization
  - Plasmid construction, lentivirus production and lentiviral transduction
  - Real-time PCR/transcriptome analyses
  - High speed video microscopy
  - Ciliary beating frequency (CBF)
  - Cilia length (CL)
  - Mucociliary transport (MCT)
  - Immunoblotting
- QUANTIFICATION AND STATISTICAL ANALYSIS

### SUPPLEMENTAL INFORMATION

Supplemental information can be found online at <https://doi.org/10.1016/j.isci.2022.104751>.

### ACKNOWLEDGMENTS

We thank Steve Brody for the help with the HSVM script. Kyle Travaglini and Mark Krasnow for their help in the analysis of the multiciliated cell transcriptome from their single-cell RNAseq database. We also thank members of the Cardoso and Lu labs at CCHD for the helpful discussions. All diagrams/illustrations in the manuscript were created with [BioRender.com](https://BioRender.com). This work was supported by NIH-NHLBI

R35-HL135834-01 to W.V.C. and Fundação para a Ciência e a Tecnologia MD PhD Scholarship PD/BD/113766/2015 to C.F.H.S.

## AUTHOR CONTRIBUTIONS

Experimental design, C.F.H.S., J.L., W.V.C.; Investigation, C.F.H.S., H.L., J.T.C., J.Q.; Resources, W.V.C.; Writing & Editing, C.F.H.S., J.L., W.V.C. Supervision, J.L., W.V.C.

## DECLARATION OF INTERESTS

The authors declare no competing interests.

Received: February 17, 2022

Revised: June 6, 2022

Accepted: July 8, 2022

Published: August 19, 2022

## REFERENCES

- Alanis, D.M., Chang, D.R., Akiyama, H., Krasnow, M.A., and Chen, J. (2014). Two nested developmental waves demarcate a compartment boundary in the mouse lung. *Nat. Commun.* 5, 3923. <https://doi.org/10.1038/ncomms4923>.
- Anderson, L.H., Boulanger, C.A., Smith, G.H., Carmeliet, P., and Watson, C.J. (2011). Stem cell marker prominin-1 regulates branching morphogenesis, but not regenerative capacity, in the mammary gland. *Dev. Dyn.* 240, 674–681. <https://doi.org/10.1002/dvdy.22539>.
- Brody, S.L., Yan, X.H., Wuerrfel, M.K., Song, S.K., and Shapiro, S.D. (2000). Ciliogenesis and left-right axis defects in forkhead factor HFH-4-null mice. *Am. J. Respir. Cell Mol. Biol.* 23, 45–51. <https://doi.org/10.1165/ajrcmb.23.1.4070>.
- Carvalho-Santos, Z., Azimzadeh, J., Pereira-Leal, J.B., and Bettencourt-Dias, M. (2011). Evolution: tracing the origins of centrioles, cilia, and flagella. *J. Cell Biol.* 194, 165–175. <https://doi.org/10.1083/jcb.201011152>.
- Choksi, S.P., Lauter, G., Swoboda, P., and Roy, S. (2014). Switching on cilia: transcriptional networks regulating ciliogenesis. *Development* 141, 1427–1441. <https://doi.org/10.1242/dev.074666>.
- Corbeil, D., Roper, K., Hannah, M.J., Hellwig, A., and Huttner, W.B. (1999). Selective localization of the polytopic membrane protein prominin in microvilli of epithelial cells - a combination of apical sorting and retention in plasma membrane protrusions. *J. Cell Sci.* 112, 1023–1033.
- Dellett, M., Sasai, N., Nishide, K., Becker, S., Papadaki, V., Limb, G.A., Moore, A.T., Kondo, T., and Ohnuma, S. (2014). Genetic background and light-dependent progression of photoreceptor cell degeneration in Prominin-1 knockout mice. *Invest. Ophthalmol. Vis. Sci.* 56, 164–176. <https://doi.org/10.1167/iov.14-15479>.
- Doench, J.G., Hartenian, E., Graham, D.B., Tothova, Z., Hegde, M., Smith, I., Sullender, M., Ebert, B.L., Xavier, R.J., and Root, D.E. (2014). Rational design of highly active sgRNAs for CRISPR-Cas9-mediated gene inactivation. *Nat. Biotechnol.* 32, 1262–1267. <https://doi.org/10.1038/nbt.3026>.
- Dubreuil, V., Marzesco, A.M., Corbeil, D., Huttner, W.B., and Wilsch-Brauninger, M. (2007). Midbody and primary cilium of neural progenitors release extracellular membrane particles enriched in the stem cell marker prominin-1. *J. Cell Biol.* 176, 483–495. <https://doi.org/10.1083/jcb.200608137>.
- Fargeas, C.A., Joester, A., Missol-Kolka, E., Hellwig, A., Huttner, W.B., and Corbeil, D. (2004). Identification of novel Prominin-1/CD133 splice variants with alternative C-termini and their expression in epididymis and testis. *J. Cell Sci.* 117, 4301–4311. <https://doi.org/10.1242/jcs.01315>.
- Florek, M., Haase, M., Marzesco, A.M., Freund, D., Ehninger, G., Huttner, W.B., and Corbeil, D. (2005). Prominin-1/CD133, a neural and hematopoietic stem cell marker, is expressed in adult human differentiated cells and certain types of kidney cancer. *Cell Tissue Res.* 319, 15–26. <https://doi.org/10.1007/s00441-004-1018-z>.
- Geling, A., Steiner, H., Willem, M., Bally-Cuif, L., and Haass, C. (2002). A gamma-secretase inhibitor blocks Notch signaling in vivo and causes a severe neurogenic phenotype in zebrafish. *EMBO Rep.* 3, 688–694. <https://doi.org/10.1093/embo-reports/kvf124>.
- Gohy, S., Carlier, F.M., Fregimilicka, C., Detry, B., Lecocq, M., Ladjemi, M.Z., Verleden, S., Hoton, D., Weynand, B., Bouzin, C., and Pilette, C. (2019). Altered generation of ciliated cells in chronic obstructive pulmonary disease. *Sci. Rep.* 9, 17963. <https://doi.org/10.1038/s41598-019-54292-x>.
- Guha, A., Vasconcelos, M., Cai, Y., Yoneda, M., Hinds, A., Qian, J., Li, G., Dickel, L., Johnson, J.E., Kimura, S., et al. (2012). Neuroepithelial body microenvironment is a niche for a distinct subset of Clara-like precursors in the developing airways. *Proc. Natl. Acad. Sci. USA.* 109, 12592–12597. <https://doi.org/10.1073/pnas.1204710109>.
- Guo, M., Du, Y., Gokey, J.J., Ray, S., Bell, S.M., Adam, M., Sudha, P., Perl, A.K., Deshmukh, H., Potter, S.S., et al. (2019). Single cell RNA analysis identifies cellular heterogeneity and adaptive responses of the lung at birth. *Nat. Commun.* 10, 37. <https://doi.org/10.1038/s41467-018-07770-1>.
- Horani, A., and Ferkol, T.W. (2018). Advances in the genetics of primary ciliary Dyskinesia: clinical implications. *Chest* 154, 645–652. <https://doi.org/10.1016/j.chest.2018.05.007>.
- Horani, A., Nath, A., Wasserman, M.G., Huang, T., and Brody, S.L. (2013). Rho-associated protein kinase inhibition enhances airway epithelial Basal-cell proliferation and lentivirus transduction. *Am. J. Respir. Cell Mol. Biol.* 49, 341–347. <https://doi.org/10.1165/rcmb.2013-0046TE>.
- Ishikawa, H., and Marshall, W.F. (2011). Ciliogenesis: building the cell's antenna. *Nat. Rev. Mol. Cell Biol.* 12, 222–234. <https://doi.org/10.1038/nrm3085>.
- Jaszai, J., Thamm, K., Karbanova, J., Janich, P., Fargeas, C.A., Huttner, W.B., and Corbeil, D. (2020). Prominins control ciliary length throughout the animal kingdom: new lessons from human prominin-1 and zebrafish prominin-3. *J. Biol. Chem.* 295, 6007–6022. <https://doi.org/10.1074/jbc.RA119.011253>.
- Karim, B.O., Rhee, K.J., Liu, G., Yun, K., and Brant, S.R. (2014). Prom1 function in development, intestinal inflammation, and intestinal tumorigenesis. *Front. Oncol.* 4, 323. <https://doi.org/10.3389/fonc.2014.00323>.
- Keeling, J., Tsiokas, L., and Maskey, D. (2016). Cellular mechanisms of ciliary length control. *Cells* 5. <https://doi.org/10.3390/cells5010006>.
- Knowles, M.R., and Boucher, R.C. (2002). Mucus clearance as a primary innate defense mechanism for mammalian airways. *J. Clin. Invest.* 109, 571–577. <https://doi.org/10.1172/JCI15217>.
- Konishi, H., Asano, N., Imatani, A., Kimura, O., Kondo, Y., Jin, X., Kanno, T., Hatta, W., Ara, N., Asanuma, K., et al. (2016). Notch1 directly induced CD133 expression in human diffuse type gastric cancers. *Oncotarget* 7, 56598–56607. <https://doi.org/10.18632/oncotarget.10967>.
- Leopold, P.L., O'Mahony, M.J., Lian, X.J., Tilley, A.E., Harvey, B.G., and Crystal, R.G. (2009). Smoking is associated with shortened airway cilia. *PLoS One* 4, e8157. <https://doi.org/10.1371/journal.pone.0008157>.

- Lopes, S.S., Lourenco, R., Pacheco, L., Moreno, N., Kreiling, J., and Saude, L. (2010). Notch signalling regulates left-right asymmetry through ciliary length control. *Development* 137, 3625–3632. <https://doi.org/10.1242/dev.054452>.
- Mall, M.A. (2016). Unplugging mucus in cystic fibrosis and chronic obstructive pulmonary disease. *Ann. Am. Thorac. Soc.* 13, S177–S185. <https://doi.org/10.1513/AnnalsATS.201509-641KV>.
- Marshall, W.F. (2008). Basal bodies platforms for building cilia. *Curr. Top. Dev. Biol.* 85, 1–22. [https://doi.org/10.1016/S0070-2153\(08\)00801-6](https://doi.org/10.1016/S0070-2153(08)00801-6).
- Marzesco, A.M., Janich, P., Wilsch-Brauninger, M., Dubreuil, V., Langenfeld, K., Corbeil, D., and Huttner, W.B. (2005). Release of extracellular membrane particles carrying the stem cell marker prominin-1 (CD133) from neural progenitors and other epithelial cells. *J. Cell Sci.* 118, 2849–2858. <https://doi.org/10.1242/jcs.02439>.
- Maw, M.A., Corbeil, D., Koch, J., Hellwig, A., Wilson-Wheeler, J.C., Bridges, R.J., Kumaramanickavel, G., John, S., Nancarrow, D., Roper, K., et al. (2000). A frameshift mutation in prominin (mouse)-like 1 causes human retinal degeneration. *Hum. Mol. Genet.* 9, 27–34. <https://doi.org/10.1093/hmg/9.1.27>.
- Mori, M., Mahoney, J.E., Stupnikov, M.R., Paez-Cortez, J.R., Szymaniak, A.D., Varelas, X., Herrick, D.B., Schwob, J., Zhang, H., and Cardoso, W.V. (2015). Notch3-Jagged signaling controls the pool of undifferentiated airway progenitors. *Development* 142, 258–267. <https://doi.org/10.1242/dev.116855>.
- Oltean, A., Schaffer, A.J., Bayly, P.V., and Brody, S.L. (2018). Quantifying ciliary dynamics during assembly reveals stepwise waveform maturation in airway cells. *Am. J. Respir. Cell Mol. Biol.* 59, 511–522. <https://doi.org/10.1165/rcmb.2017-0436OC>.
- Polin, R.A. (2011). *Fetal and Neonatal Physiology* (Saunders).
- Qiu, Z.X., Zhao, S., Mo, X.M., and Li, W.M. (2015). Overexpression of PROM1 (CD133) confers poor prognosis in non-small cell lung cancer. *Int. J. Clin. Exp. Pathol.* 8, 6589–6595.
- Rawlins, E.L., and Hogan, B.L. (2008). Ciliated epithelial cell lifespan in the mouse trachea and lung. *Am. J. Physiol. Lung Cell Mol. Physiol.* 295, L231–L234. <https://doi.org/10.1152/ajplung.90209.2008>.
- Rock, J.R., Onaitis, M.W., Rawlins, E.L., Lu, Y., Clark, C.P., Xue, Y., Randell, S.H., and Hogan, B.L. (2009). Basal cells as stem cells of the mouse trachea and human airway epithelium. *Proc. Natl. Acad. Sci. USA.* 106, 12771–12775. <https://doi.org/10.1073/pnas.0906850106>.
- Sanjana, N.E., Shalem, O., and Zhang, F. (2014). Improved vectors and genome-wide libraries for CRISPR screening. *Nat. Methods* 11, 783–784. <https://doi.org/10.1038/nmeth.3047>.
- Sansone, P., Berishaj, M., Rajasekhar, V.K., Ceccarelli, C., Chang, Q., Strillacci, A., Savini, C., Shapiro, L., Bowman, R.L., Mastroleo, C., et al. (2017). Evolution of cancer stem-like cells in endocrine-resistant metastatic breast cancers is mediated by stromal microvesicles. *Cancer Res.* 77, 1927–1941. <https://doi.org/10.1158/0008-5472.CAN-16-2129>.
- Schindelin, J., Arganda-Carreras, I., Frise, E., Kaynig, V., Longair, M., Pietzsch, T., Preibisch, S., Rueden, C., Saalfeld, S., Schmid, B., et al. (2012). Fiji: an open-source platform for biological-image analysis. *Nat. Methods* 9, 676–682. <https://doi.org/10.1038/nmeth.2019>.
- Shmelkov, S.V., Butler, J.M., Hooper, A.T., Hormigo, A., Kushner, J., Milde, T., St Clair, R., Baljevic, M., White, I., Jin, D.K., et al. (2008). CD133 expression is not restricted to stem cells, and both CD133+ and CD133- metastatic colon cancer cells initiate tumors. *J. Clin. Invest.* 118, 2111–2120. <https://doi.org/10.1172/JCI34401>.
- Singer, D., Thamm, K., Zhuang, H., Karbanova, J., Gao, Y., Walker, J.V., Jin, H., Wu, X., Coveney, C.R., Marangoni, P., et al. (2019). Prominin-1 controls stem cell activation by orchestrating ciliary dynamics. *EMBO J.* 38. <https://doi.org/10.15252/embj.201899845>.
- Singla, V., and Reiter, J.F. (2006). The primary cilium as the cell's antenna: signaling at a sensory organelle. *Science* 313, 629–633. <https://doi.org/10.1126/science.1124534>.
- Sisson, J.H., Stoner, J.A., Ammons, B.A., and Wyatt, T.A. (2003). All-digital image capture and whole-field analysis of ciliary beat frequency. *J. Microsc.* 211, 103–111. <https://doi.org/10.1046/j.1365-2818.2003.01209.x>.
- Stasiulewicz, M., Gray, S.D., Mastromina, I., Silva, J.C., Bjorklund, M., Seymour, P.A., Booth, D., Thompson, C., Green, R.J., Hall, E.A., et al. (2015). A conserved role for Notch signaling in priming the cellular response to Shh through ciliary localisation of the key Shh transducer Smo. *Development* 142, 2291–2303. <https://doi.org/10.1242/dev.125237>.
- Stupnikov, M.R., Yang, Y., Mori, M., Lu, J., and Cardoso, W.V. (2019). Jagged and Delta-like ligands control distinct events during airway progenitor cell differentiation. *Elife* 8. <https://doi.org/10.7554/eLife.50487>.
- Tinevez, J.Y., Perry, N., Schindelin, J., Hoopes, G.M., Reynolds, G.D., Laplantine, E., Bednarek, S.Y., Shorte, S.L., and Eliceiri, K.W. (2017). TrackMate: an open and extensible platform for single-particle tracking. *Methods* 115, 80–90. <https://doi.org/10.1016/j.ymeth.2016.09.016>.
- Toskala, E., Smiley-Jewell, S.M., Wong, V.J., King, D., and Plopper, C.G. (2005). Temporal and spatial distribution of ciliogenesis in the tracheobronchial airways of mice. *Am. J. Physiol. Lung Cell Mol. Physiol.* 289, L454–L459. <https://doi.org/10.1152/ajplung.00036.2005>.
- Travaglini, K.J., Nabhan, A.N., Penland, L., Sinha, R., Gillich, A., Sit, R.V., Chang, S., Conley, S.D., Mori, Y., Seita, J., et al. (2020). A molecular cell atlas of the human lung from single-cell RNA sequencing. *Nature* 587, 619–625. <https://doi.org/10.1038/s41586-020-2922-4>.
- Tsai, W.-H. (1985). Moment-preserving thresholding: a new approach. *Comput. Vis. Graph Image Process* 29, 377–393. [https://doi.org/10.1016/0734-189X\(85\)90133-1](https://doi.org/10.1016/0734-189X(85)90133-1).
- Tsao, P.N., Vasconcelos, M., Izvolzky, K.I., Qian, J., Lu, J., and Cardoso, W.V. (2009). Notch signaling controls the balance of ciliated and secretory cell fates in developing airways. *Development* 136, 2297–2307. <https://doi.org/10.1242/dev.034884>.
- Tsao, P.N., Wei, S.C., Wu, M.F., Huang, M.T., Lin, H.Y., Lee, M.C., Lin, K.M., Wang, I.J., Kaartinen, V., Yang, L.T., and Cardoso, W.V. (2011). Notch signaling prevents mucous metaplasia in mouse conducting airways during postnatal development. *Development* 138, 3533–3543. <https://doi.org/10.1242/dev.063727>.
- Weigmann, A., Corbeil, D., Hellwig, A., and Huttner, W.B. (1997). Prominin, a novel microvilli-specific polytopic membrane protein of the apical surface of epithelial cells, is targeted to plasmalemmal protrusions of non-epithelial cells. *Proc. Natl. Acad. Sci. USA.* 94, 12425–12430. <https://doi.org/10.1073/pnas.94.23.12425>.
- You, Y., and Brody, S.L. (2013). Culture and differentiation of mouse tracheal epithelial cells. *Methods Mol. Biol.* 945, 123–143. [https://doi.org/10.1007/978-1-62703-125-7\\_9](https://doi.org/10.1007/978-1-62703-125-7_9).
- You, Y., Richer, E.J., Huang, T., and Brody, S.L. (2002). Growth and differentiation of mouse tracheal epithelial cells: selection of a proliferative population. *Am. J. Physiol. Lung Cell Mol. Physiol.* 283, L1315–L1321. <https://doi.org/10.1152/ajplung.00169.2002>.
- You, Y., Huang, T., Richer, E.J., Schmidt, J.E., Zabner, J., Borok, Z., and Brody, S.L. (2004). Role of f-box factor foxj1 in differentiation of ciliated airway epithelial cells. *Am. J. Physiol. Lung Cell Mol. Physiol.* 286, L650–L657. <https://doi.org/10.1152/ajplung.00170.2003>.

STAR★METHODS

KEY RESOURCES TABLE

| REAGENT or RESOURCE   | SOURCE   | IDENTIFIER   |
|---|--|--|
| <b>Antibodies</b>   |  |  |
| Rat monoclonal anti-CD133 (Prominin-1) (clone 13A4)   | Thermo Fisher Scientific   | Cat#14-1331-82; RRID: AB_467471  |
| Mouse monoclonal anti-FOXJ1 (clone 2A5)   | Thermo Fisher Scientific   | Cat#14-9965-80; RRID: AB_1548836   |
| Rabbit monoclonal anti-Acetyl- $\alpha$ -Tubulin (clone D20G3)                                | Cell Signaling Technology  | Cat#5335; RRID: AB_10544694  |
| Mouse monoclonal anti-beta IV Tubulin (clone ONS.1A6)   | Abcam  | Cat#ab11315; RRID: AB_297919   |
| Mouse monoclonal anti-CETN3 (clone 3E6)   | Abnova   | Cat#H00001070-M01; RRID: AB_464016   |
| Rabbit monoclonal anti-p62- $\alpha$ (clone D2K8K)  | Cell Signaling Technology  | Car#13109; RRID: AB_2637091  |
| Rabbit monoclonal anti-RBPSUH (clone D10A4)   | Cell Signaling Technology  | Cat#5313; RRID: AB_2665555   |
| Rat monoclonal anti-Mouse Ugrp1 (clone 381707)  | R and D Systems  | Cat#MAB3465; RRID: AB_2183548  |
| Goat polyclonal anti-CC10 (clone T-18)  | Santa Cruz Biotechnology   | Cat#sc-9772; RRID: AB_2238819  |
| Rabbit monoclonal anti-Notch1, cleaved (Val1744) (clone D3B8)                                 | Cell Signaling Technology  | Cat#4147; RRID: AB_2153348   |
| <b>Chemicals, peptides, and recombinant proteins</b>  |  |  |
| TransIT-293 Transfection Reagent  | Mirus Bio  | Cat#2700   |
| ROCK Inhibitor (Y-27632)  | Sigma-Aldrich  | Cat#SCM075   |
| DAPT  | Sigma-Aldrich  | Cat#D5942  |
| <b>Deposited data</b>   |  |  |
| Transcriptome analyses  | <a href="#">Tsao et al. (2009)</a> ;<br><a href="#">Guha et al. (2012)</a> | GEO: GSE52926  |
| <b>Experimental models: Cell lines</b>  |  |  |
| Air-Liquid Interface (ALI) organotypic airway epithelial culture                              | Generated from Wild Type C57BL/6   | N/A  |
| HEK293T   | N/A  | RRID: CVCL_0063  |
| <b>Experimental models: Organisms/strains</b>   |  |  |
| Mouse: Wild Type C57BL/6  | Charles River  | Strain code: 027   |
| Mouse: ShhCre; Rbpjk <sup>flf</sup>   | <a href="#">Tsao et al. (2009)</a>   | N/A  |
| Mouse: ShhCre; NICD   | <a href="#">Guha et al. (2012)</a>   | N/A  |
| <b>Oligonucleotides</b>   |  |  |
| sgRNA spacer sequence: Prom1: TGAGCAGACAAATCACCAGG  | This paper   | N/A  |
| sgRNA spacer sequence: Prom1: TGGGGGTCTGTGCCTCCTGG  | This paper   | N/A  |
| Prom1 <i>in situ</i> hybridization forward primer: AATTAACCCTCACTAAAGGGCTTTGAGTGAATGACCACCTTG | This paper   | N/A  |
| Prom1 <i>in situ</i> hybridization reverse primer: TAATACGACTCACTATAGGGGCTTGAATCAACTGAGATGTC  | This paper   | N/A  |
| <b>Recombinant DNA</b>  |  |  |
| lentiCRISPR v2  | <a href="#">Sanjana et al. (2014)</a>                                      | Addgene Plasmid #5296; 1RRID: Addgene_52961  |
| MGC Mouse Prom1 cDNA (clone: 4502359)   | Dharmacon (now Horizon Discovery)  | Cat#MMM4769-202766484  |
| <b>Software and algorithms</b>  |  |  |
| Fiji  | <a href="#">Schindelin et al. (2012)</a>                                   | <a href="https://fiji.sc/">https://fiji.sc/</a> ; RRID: SCR_002285                 |
| GraphPad Prism  | GraphPad   | <a href="http://www.graphpad.com/">http://www.graphpad.com/</a> ; RRID: SCR_002798 |

(Continued on next page)

**Continued**

| REAGENT or RESOURCE  | SOURCE  | IDENTIFIER  |
|--|---|---|
| sgRNA Design v1  | Doench et al. (2014)                                    | <a href="http://www.broadinstitute.org/mal/public/analysis-tools/sgna-design-v1">http://www.broadinstitute.org/mal/public/analysis-tools/sgna-design-v1</a> |
| CoreView   | IO Industries   | <a href="https://www.ioindustries.com/">https://www.ioindustries.com/</a>   |
| MATLAB   | MathWorks   | <a href="http://www.mathworks.com/products/matlab/">http://www.mathworks.com/products/matlab/</a> ; RRID:SCR_001622   |
| TrackMate  | Tinevez et al. (2017)                                   | <a href="https://imagej.net/plugins/trackmate/">https://imagej.net/plugins/trackmate/</a>   |
| <b>Other</b>   |   |   |
| Protocol: Target Guide Sequence Cloning  | Zhang Lab   | <a href="https://www.addgene.org/crispr/reference/#protocols">https://www.addgene.org/crispr/reference/#protocols</a>                                       |
| Protocol: Packaging of VSV-G Pseudotyped Lentivirus by 5 Plasmid Co-Transfection of 293T cells | The Center for Regenerative Medicine, Boston University | <a href="https://crem.bu.edu/cores-protocols">https://crem.bu.edu/cores-protocols</a>   |
| Protocol: Culture and Differentiation of Mouse Tracheal Epithelial Cells                       | You and Brody (2013)                                    | N/A   |

**RESOURCE AVAILABILITY****Lead contact**

Further information and requests for resources and reagents should be directed to and will be fulfilled by the lead contact, Wellington V. Cardoso ([wvc2104@cumc.columbia.edu](mailto:wvc2104@cumc.columbia.edu)).

**Materials availability**

This study did not generate new unique reagents.

**Data and code availability**

- All data reported in this paper will be shared by the [lead contact](#) upon request.
- This paper does not report original code.
- Any additional information required to reanalyze the data reported in this paper is available from the [lead contact](#) upon request.

**EXPERIMENTAL MODEL AND SUBJECT DETAILS****Mouse models**

*Rbpjk<sup>cnul</sup>* and *ShhCre;NICD* mice were generated as described by Tsao et al. (2009) and Guha et al. (2012). The male *Shh<sup>Cre/+</sup>;Rbpjk<sup>+/-</sup>*, female *Rbpjk<sup>F/F</sup>*, male *Shh<sup>Cre/+</sup>;Pofut1<sup>+/-</sup>*, female *ROSA26-NICD-IRES-GFP*, and wild-type control mice were kept under pathogen free and controlled lighting (12h cycles) conditions. The mice were housed in individually-ventilated, HEPA-filtered cages (maximum of five adults per cage), and all handling occurred in HEPA-filtered biosafety hoods. Mice were provided with normal chow and water *ad libitum*. For embryonic stages, the detection of vaginal plugs in the morning was considered as day 0.5, and embryos were harvested at either E14.5 or E18.5. All experiments were approved by Columbia University Institutional Animal Care and Use Committee (IACUC).

**Air-liquid-interface (ALI) organotypic airway epithelial cultures**

Mouse tracheal epithelial cells were isolated from the tracheas of adult (8–12 weeks old) male C56BL/6J mice and released from tissue by pronase digestion (1.5 mg/mL) for 24 h at 4°C. Airway epithelial cells were isolated from fibroblasts by differential adhesion, as previously described by You and Brody (2013). Freshly isolated mTEC were seeded at a density of  $1 \times 10^5/\text{cm}^2$  on supported semi-permeable polyester membranes (Transwell, Corning) that had previously been coated with collagen. The medium used to initiate the cell culture was mTEC/Plus supplemented with 10% FBS and retinoic acid. Once the cells were confluent (day 0), and to induce their differentiation, the medium from the upper chamber was aspirated, thereby inducing an air-liquid-interface (ALI), and the medium from the bottom chamber was replaced with mTEC/Serum-Free (mTEC/Basic) supplemented with retinoic acid, as previously described (You and Brody, 2013). Cell cultures were maintained by replacing the respective media every 48h or

less, for up to 27 days after inducing the air-liquid interface. For genetic disruption of Notch signaling in mTEC ALI cultures, adult basal cells from *Rbpjk<sup>flox/flox</sup>* mice were isolated and transduced with a lentivirus-expressing Cre as we previously reported (Mori et al., 2015). For Notch pharmacological inhibition, mTEC were cultured from ALI day -3 to ALI day 8 with an added gamma-secretase inhibitor (DAPT, 50  $\mu$ M, Sigma) or vehicle control (DMSO, Sigma, D8418), as previously described.

## METHOD DETAILS

### Immunofluorescence (IF)

Whole E14.5 embryos and E18.5 lungs and tracheas were fixed overnight at 4°C in 4% paraformaldehyde, processed for frozen OCT embedding and sectioned (5  $\mu$ m) in a cryotome, as previously reported (Stupnikov et al., 2019). Transwell membranes of ALI airway organotypic cultures were fixed with 4% paraformaldehyde for 10 min at room temperature and processed as described by You et al. (2002). For IF, tissue sections were incubated overnight at 4°C with primary antibody, while for Transwell membranes antibody incubation was performed at room temperature for 2 h. For NICD detection in E18.5 lung frozen sections, IF signals were detected using a TSA Cyanine 3 (Cy3) reagent kit (Akoya Biosciences #SAT704A001EA), according to manufacturer's instructions. For all other samples, IF signals were detected using Alexa Fluor 488, Alexa Fluor 568, or Alexa 647-labeled secondary antibodies (1:250) (Thermo Fisher Scientific) for 2 h at room temperature. 4',6-diamidino-2-phenylindole (DAPI) was used to stain intracellular DNA (NucBlue, Thermo Fisher Scientific). Alexa Fluor 647 Phalloidin (Thermo Fisher Scientific) was used to visualize filamentous actin (F-actin). Following PBS washes, tissue sections and membranes were mounted with anti-fade mounting media (Pro-Long Gold, Thermo Fisher Scientific) and examined. The antibodies used were: anti-CD133 (Prominin-1) (Thermo Fisher Scientific #14-1331-82, 1:100), anti-Foxj1 (Thermo Fisher Scientific #14-9965-80, 1:100), anti-Acetyl- $\alpha$ -Tubulin (Cell Signaling Technology #5335, 1:300), anti-beta IV Tubulin (Abcam #ab11315, 1:100), anti-Cetn3 (Abnova #H00001070-M01, 1:50), anti-p63- $\alpha$  (Cell Signaling Technology #13109, 1:100), anti-RBPSUH (Cell Signaling Technology #5313, 1:100), anti-UGRP1 (R and D Systems, #MAB3465, 1:100), anti-Cc10 (Santa Cruz Biotechnology #sc-9772, 1:100), and anti-cleaved Notch1 (Cell Signaling Technology #4147, 1:100). Confocal laser scanning micrographs were acquired using a Zeiss LSM-710 laser scanning microscope (Zeiss) equipped with a motorized stage, 20x dry or 63x oil-immersion objectives, and an argon laser. For z stack analysis, the Z-stepper was configured to take 130 nm steps. The remaining fluorescent micrographs were taken with a Leica DMI8 widefield fluorescence microscope (Leica Microsystems), and a 40x dry objective.

### Cytometry and fluorescence intensity analyses

#### Analyses of Prom1 fluorescence intensity

We performed Prom1 immunostaining of E18.5 tracheas and lungs from control and *Rbpjk<sup>cnull</sup>* mutant mice. The intensity of fluorescence detection was evaluated in maximum projections representative of different airway generations (trachea, primary bronchus, secondary bronchus and bronchiole) from a single E18.5 section by setting an automatic threshold (Tsai, 1985) that limited the ROI to the areas where Prom1 signal was detected, and then calculating, for five individual cells per field, the mean gray value and its SD with the Fiji software (Schindelin et al., 2012). The measurements were normalized as a percentage of the mean fluorescence values of the trachea (set as 100%), and plotted on a bar chart with a beeswarm plot superimposed.

For our analysis of airway epithelial cultures, we performed Prom1 immunostaining and F-actin labeling with fluorescent Phalloidin in ALI day 0 and ALI day 8 mouse airway epithelial cell cultures. The samples were obtained from mouse tracheal epithelial cells that had been incubated with the gamma-secretase inhibitor DAPT, or DMSO for vehicle controls, from 3 days prior to confluence being reached (ALI day -3). The intensity of fluorescence detection was evaluated in single representative sum of slices projections by delimiting the cell borders evidenced by Phalloidin with the Polygon tool, and calculating the mean gray value (MGV) and integrated density (MGV  $\times$  Cell area) of Prom1 detection in each Prom1-labelled individual cell ( $126 < N_{\text{cells}} < 272$ ) with the Fiji software (Schindelin et al., 2012). The MGV of Prom1 were normalized by those of fluorescent Phalloidin, and so that the average MGV or integrated density of controls (DMSO) equaled 100% for each stage (days 0 and 8). The normalized Prom1 integrated densities in sum of slices projections (labeled "total fluorescence") from both stages were plotted on vertical violin plots together with the respective mean, median, and quartiles. The frequency distributions of normalized MGV (with a bin width of 10) from day 8 were curve-fitted with non-linear regression (Gaussian or sum of two

Gaussians), and plotted on a bar chart together with the best fitting curve, the mean of the sample, and the mean of the respective best fitting Gaussian or sum of Gaussian curves.

### Cytometric analyses

Quantitative assessment of Foxj1-positive cells was performed in ALI day 8 mouse airway epithelial cell cultures that had been transduced with a lentivirus containing either an sgRNA sequence targeting Foxj1 (Foxj1 KO), or a scrambled sgRNA sequence (control). The number of Foxj1-positive cells was measured in 10 random fields for each condition by using the Multi-point tool of the Fiji software (Schindelin et al., 2012). The individual values were plotted in a beeswarm plot with the sample-mean and respective SD superimposed.

Quantitative assessment of p63-positive cells was performed in ALI day 0 mouse airway epithelial cell cultures that had been transduced with a lentivirus containing either an sgRNA sequence targeting Prom1 (Prom1 KO), or a scrambled sgRNA sequence (control). The number of p63-positive cells was measured in 20 random fields from three independent ALI culture wells for each condition, by using the Multi-point tool of the Fiji software (Schindelin et al., 2012). The individual values and the well-means were plotted as a beeswarm plot with the sample-mean and respective SD superimposed.

Cetn3-positive cells were quantified in ALI day 4 mouse airway epithelial cell cultures transduced with a lentivirus containing Prom1 KO or a control sgRNA sequence. The number of Cetn3-positive cells was measured in 20 random fields from three independent ALI culture wells for each condition, by using the Analyze Particles tool of the Fiji software (Schindelin et al., 2012). The individual values and the well-means were plotted as a beeswarm plot with the sample-mean and respective SD superimposed.

### In situ hybridization

*In situ* hybridization was performed in frozen sections as we previously described in Tsao et al. (2009). The hybridization probe was synthesized from a Mammalian Gene Collection (MGC) fully sequenced mouse Prom1 cDNA (4502359, Dharmacon). After confirmation by Sanger sequencing, the plasmid was linearized, and then amplified with Q5 High-fidelity DNA polymerase (M0491S, New England Biolabs) according to the manufacturer's instructions. The forward primer used was AATTAACCCTCACTAAA GGGCTTTGAGTGAATGACCACCTTG and the reverse primer was TAATACGACTCACTATAGGG GCCTTGAATCAACTGAGATGTC. The PCR product was transcribed with QIAquick PCR Purification Kit (#28104, Qiagen), transcribed with MAXIscript Kit (#AM1320, Thermo Fisher Scientific), and purified with RNeasy MinElute Cleanup Kit (#74204, Qiagen), according to manufacturer's instructions.

### Plasmid construction, lentivirus production and lentiviral transduction

Three sgRNAs targeting the Prom1 gene and three sgRNAs targeting the Foxj1 gene were designed and selected according to their predicted sgRNA efficient scores, as calculated by the sgRNA designer tool provided by Broad Institute (available at: <http://www.broadinstitute.org/rnai/public/analysis-tools/sgrna-design-v1>) that implements the Rule Set one sgRNA scoring algorithm described in Doench et al. (2014). A scrambled-sequence sgRNA was designed to serve as a negative control. The sgRNA oligos were cloned into lentiCRISPRv2 plasmid (Sanjana et al., 2014) as previously described in the Target Guide Sequence Cloning Protocol from the Zhang Lab (available at: <https://www.addgene.org/crispr/reference/#protocols>). Each plasmid containing an inserted sgRNA sequence was verified using Sanger sequencing.

The VSV-G pseudotyped lentivirus was packaged by five plasmid co-transfection of HEK293T cells using TansIT-293 Transfection Reagent (#2700, Mirus Bio) in 15 cm culture dishes (The protocol describing production of lentiviral particles can be found at <https://crem.bu.edu/cores-protocols/>). HEK293T cells were cultured in high glucose DMEM medium containing 10% FBS. The supernatant was collected for a total of 5 times, starting at 48 h after transfection and every 12 h afterwards, and readily filtered with a 0.45  $\mu$ m pore size vacuum filter. The filtrate was concentrated by spinning for 90 min at 48,000 g, resuspended in high glucose DMEM medium, and stored at  $-80^{\circ}\text{C}$ .

For lentiviral transduction, the protocol outlined by Horani et al. (2013) was used. Following the isolation by differential adhesion, mouse airway epithelial cells were resuspended in mTEC/Plus supplemented with retinoic acid, Polybrene, and 10 mM Y-27632. At this point, 10  $\mu$ L of concentrated lentivirus filtrate were added to a 1.5 mL microfuge tube containing 150  $\mu$ L of resuspended cells. After 10 min of incubation at

room temperature, the cells were delivered to the apical surface of the supported membranes. After 24 h of incubation at 37°C, the culture medium was aspirated from the bottom chamber only, and replaced with fresh mTEC/Plus supplemented with retinoic acid and Y27632. In order to maximize adhesion, the medium on the upper chamber was not aspirated for the first 48 h after transduction, at which time it was replaced with fresh mTEC/Plus supplemented with retinoic acid and Y27632. Starting 72 h after the initial exposure to the lentivirus, the culture medium was supplemented with 2.0 µg/mL puromycin for two consecutive 48 h periods, resulting in a total of 4 days of puromycin treatment. The culture medium (mTEC/Plus) was supplemented with Y27632 for the entire duration of the submerged conditions, which was only discontinued when the medium from the upper chamber was aspirated and the air-liquid interface induced (ALI day 0). The sgRNA with the highest expression-disrupting efficiency for each gene, as assessed by cytometric analysis of immunofluorescence for Prom1 at ALI day 0, or Foxj1 at ALI days 4 and 8, was used in subsequent experiments. The sgRNA sequence used for the targeted disruption of Prom1 was TGAGCAGACAAATCACCAGG. The sgRNA sequence used for the targeted disruption of Foxj1 was TGGGGTCTGTGCCTCTGG. Generation of Lentivirus-expressing Cre and expression in ALI cultures were previously reported (Mori et al., 2015).

### Real-time PCR/transcriptome analyses

For quantitative real-time PCR analysis of the organotypic airway cultures Transwell membranes containing mTEC-derived cells were cut from the supporting structure and submerged in RLT lysis buffer. RNA was extracted with an RNeasy Mini kit (#74106, Qiagen), according to the manufacturer's instructions. First-strand cDNA was synthesized with the Super-Script IV First-Strand Synthesis System (#18091050, Thermo Fisher Scientific), according to the manufacturer's instructions. Quantitative RT-PCR was performed as previously described by using Taq-Man Advanced Master Mix (#4444556, Thermo Fisher Scientific) and a StepOnePlus™ Real-Time PCR System (Applied Biosystems). The following primers (Thermo Fisher Scientific) were used: Prom1 (Mm01211402\_m1), Foxj1 (Mm01267279\_m1), Scgb3a2 (Mm00504412\_m1) and Cetn3 (Mm00514305\_m1). ACTB was used as an internal control. The changes in expression levels were calculated using the  $\Delta\Delta C_t$  method. The results were either plotted as Relative Expression Levels (Fold Change  $\pm$  CI95) in a bar chart, or as  $\Delta C_t$  ( $C_{t_{\text{target}}} - C_{t_{\text{ACTB}}}$ ) in a beeswarm plot with the mean  $\pm$  SD superimposed. Regarding the latter, a lower  $\Delta C_t$  corresponds to decreased expression of the target gene. Transcriptome analysis was previously performed in E18.5 WT, Rbpjk<sup>cnul</sup>, ShhCre; NICD1 (Guha et al., 2012; Tsao et al., 2009) and deposited (GEO: GSE52926).

### High speed video microscopy

Mouse tracheal epithelial cells cultured *in vitro* on supported membranes were imaged live with a 40× objective on a live cell-configured inverted microscope (Axio Observer Z1 platform equipped with Apo-Tome.2, Zeiss) attached to a high-speed video camera in order to capture an *en face* view of distal tips of beating cilia. Videos were captured in 25 random locations in each membrane. ALI cultures were also scraped so that clusters of ciliated cells could be placed on a microscope slide and the cilia viewed from the side. To achieve this, 20 µL of culture medium were added to the surface of the ALI cultures, a small area of cells scraped with a 200 µL micropipette-tip, and the cells suspended in medium and transferred to a microscope slide, as previously described by Oltean et al. (2018). All cells were imaged inside a live cell-imaging chamber heated to a stable temperature of 37°C, at a frame rate of 360 frames per second, and for a duration of at least 720 frames using CoreView (v2.2.0.9) software (IO Industries). Mucociliary transport was assessed by tracking the displacement of microspheres added to the apical surface of live ALI cultures. The cultures were imaged under conditions similar to the above, but with a 10× objective, a fluorescent light source, and at a frame rate of 25 frames per second, as previously described by Oltean et al. (2018). Videos were captured in five random locations in each membrane.

### Ciliary beating frequency (CBF)

CBF was calculated from *en face* video recordings of mTEC cultured on supported membranes and of scraped multiciliated cells placed on microscope slides. CBF was calculated for each video by using the fast Fourier transform (FFT) in MATLAB (R2019a, Mathworks), as previously described by Oltean et al. (2018). In order to quantify the CBF across each video frame, the frequency of the highest magnitude peak in the FFT was identified for each pixel. Only pixels in which the FFT indicated a magnitude greater than 1, in units of pixel intensity, and frequency greater than or equal to 2 Hz were included in the CBF heatmap and used to calculate the video average, as originally described by Sisson et al. (2003). The averages

from each video and the well-means were plotted as a beeswarm plot with the sample-mean and respective SD superimposed.

### Cilia length (CL)

CL was assessed in adult mTEC cultures in multiciliated cells scraped from the membranes and placed on microscope slides. Damaged cilia, or those in proximity to other cells and/or debris were excluded. Five individual cilia per multiciliated cell were measured and the average cilia length per cell ( $\mu\text{m}$ ) was determined. The cell-means and well-means were plotted as a beeswarm plot superimposed on a bar chart representing the sample-means and respective standard deviations. The means were compared using a two-tailed unpaired t-test (Prism 8.4.3 software, GraphPad). In the experiments involving lenti-Cre transduction of WT or *Rbpjk<sup>fl/fl</sup>* ALI cultures CL was assessed in ten individual cilia from a representative confocal laser scanning micrograph of each condition using Zeiss LSM imager browser. Sample-means were plotted in a bar chart with their respective standard deviations and differences were compared using a two-tailed unpaired t-test. In a subset of multiciliated cells from control ALI cultures CL and CBF were analyzed simultaneously. The correlation between these two variables was analyzed by computing Pearson correlation coefficients (two-tailed, alpha of 0.05) using a simple linear regression. The CL and CBF pairs were plotted in a scatterplot with the linear regression line (solid) and CI 95 (dashed) superimposed.

### Mucociliary transport (MCT)

MCT was assessed by automatically tracking the displacement of fluorescent microspheres (1  $\mu\text{m}$  diameter, Fluoro Max Dyed Green, G0100, Thermo Fisher Scientific) added to the surface of live ALI cultures by using the Fiji plugin TrackMate (Tinevez et al., 2017). The solution of microspheres was diluted 1:1,000 in PBS, approximately 15  $\mu\text{L}$  of the diluted microsphere solution was added to the surface of the ALI, and the culture plates returned to the incubator for approximately 10–40 min prior to imaging, as previously described by Oltean et al. (2018). The final MCT value was calculated by weight-averaging the track displacement velocity by the track displacement distance, thereby accounting for microspheres that may have gone in- and out-of-focus as well as for microspheres that may have only briefly crossed the microscope field. The averages from each video and the well-means were plotted as a beeswarm plot with the sample-mean and respective SD superimposed.

### Immunoblotting

For immunoblotting analysis of Prom1, mouse airway epithelial cells grown on permeable supported membranes were washed at ALI day 0 with cold PBS and scraped off. The samples were obtained from the proliferation of mouse tracheal epithelial cells that had been transduced with a lentivirus containing either an sgRNA sequence targeting Prom1 (Prom1 KO) or a scrambled sgRNA sequence (control). Proteins were analyzed by SDS-polyacrylamide gel electrophoresis (SDS-PAGE, 12%), and transferred to Immobilon-P PVDF Membrane (IPVH00010, Millipore), according to standard procedures. Immunoblotting was performed as previously described by Corbeil et al. (1999), using anti-CD133 (Prominin-1) (Thermo Fisher Scientific #14-1331-82) as a primary antibody.

## QUANTIFICATION AND STATISTICAL ANALYSIS

Information on sample sizes, and statistical tests used with respective p value interval is provided in the respective figure's legend. Shapiro-Wilk (Figure 1) or D'Agostino & Pearson (all others) tests were used to test for normal distribution (alpha = 0.05); normality was assumed for qPCR and microarray data. *F*-tests were used to compare the variances of two groups (alpha = 0.05). Student's unpaired t-tests were used when the unpaired data of two groups was normally distributed and had equal variances (alpha = 0.05); Welch's unpaired t-tests were used when the variances were not equal (alpha = 0.05). Mann Whitney tests were used when unpaired data of two groups was not normally distributed (alpha = 0.05). Ordinary one-way ANOVA, with either Sidak's or Dunnett's post-hoc comparison tests (family-wise alpha = 0.05) were used when the data from more than two groups was normally distributed. All statistical analyses were performed with Prism 8.4.3 software (GraphPad).